Available online at www.sciencedirect.com
ScienceDirect
Polymer 47 (2006) 8106–8115
polymer
www.elsevier.com/locate/polymer

Nanoclay reinforced bio-based elastomers: Synthesis and characterization

Lin Zhu, Richard P. Wool*

Department of Chemical Engineering, University of Delaware, Newark, DE 19716, USA

Received 15 November 2005; received in revised form 24 July 2006; accepted 28 July 2006
Available online 16 October 2006

Abstract

A new bio-based elastomer synthesized from soybean oil was filled with nanoclay to generate an elastic nanocomposite. A solubility parameter study was used to select the organoclay for poly(acrylated oleic methyl ester) (AOME). Effects of the nanoclay on the macroscopic and microscopic properties were explored. The morphology varies from fully exfoliated to intercalated structure with different types of clay and clay concentrations. Mechanical properties are significantly improved by the addition of organoclays. The elongation at break increases as well as the tensile strength. A decrease in the crosslink density of this elastic nanocomposite, measured by swelling test, indicates that the clay hinders chemical crosslinking and also confirms the formation of physical crosslinks. Percolation studies show the improvement of the network structure by nanoclays. The onset of the thermal decomposition was hindered by the loading of the nanoclay. Clay effects on biodegradability were studied as well.

Keywords: Polymer layered silicate; Renewable resources; Elastomers

1. Introduction

Clay is widely used as a non-black filler in the rubber industry. It is noted for its low cost and low-to-moderate reinforcement [1]. In recent years, this traditional filler attracted considerable interest when layered silicates were dispersed in a polymer matrix at the nano-scale level and the reinforcement ability was significantly improved. In 1987, the Toyota research group [2] replaced the inorganic exchange cations in the galleries of the native clay by alkylammonium surfactants and first applied it to the ring opening nylon polymerization. The surface chemistry of the modified clay was compatible with the hydrophobic polymer matrix and agglomeration disappeared. Over the past decade, the combinations of polymers and nanofillers have shown great opportunities to form nanocomposites with dramatically improved mechanical and thermal properties [3]. The research on organoclay reinforced nanocomposites has been extended to epoxy resins [4–12], polyamide [6,13–16], polystyrene [17–20], polyurethane [21–23], polypropylene [24–26], polyester [27–30], etc. These nanocomposites demonstrate improvements in tensile properties, gas barrier action, thermal stability and flame retardation [3].

Nanoclay has also been utilized in the field of elastomers [31–41]. Kojima et al. [31] studied nanoclay reinforced nitrile rubber and found that the permeability of hydrogen and water vapor is reduced by about one-third. Lopez-Manchado et al. [32–34] prepared organoclay nanocomposites based on natural rubber and noticed an increase in the crosslink density, degree of curing, structure order and glass transition temperature. *cis*-1,4-Polyisoprene and epoxidized natural rubber were studied by Vu and coworkers [35]. Clays were incorporated into the elastomers by mixing the components in a standard internal blender or by mixing dispersions of them in toluene or methyl ethyl ketone. They found that the reinforcing effects depend on the degree of exfoliation. Morphology and mechanical properties of clay reinforced styrene–butadiene rubber were explored by Zhang et al. [36]. SBR latex was mixed

* Corresponding author. Tel.: +1 302 831 3312; fax: +1 302 831 1048.
E-mail address: wool@udel.edu (R.P. Wool).

0032-3861/$ - see front matter © 2006 Elsevier Ltd. All rights reserved.
doi:10.1016/j.polymer.2006.07.076

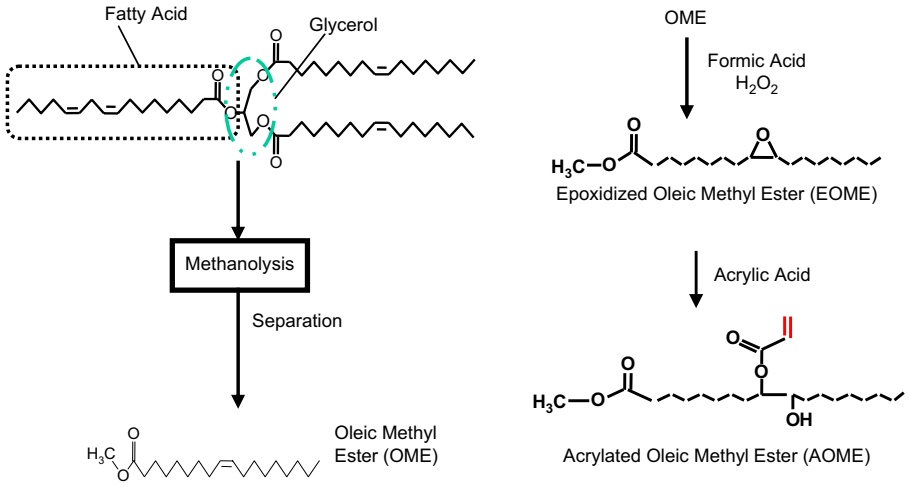

Fig. 1. Structure of triglycerides and synthesis of acrylated oleic methyl ester monomer from triglyceride [59].

with a clay/water dispersion to achieve the structure of layered bundles. The mechanical properties were increased when compared with other fillers and regular rubber processing methods of mixing. Wang et al. [37] synthesized silicone rubber/organo-montmorillonite hybrid nanocomposites by the melt intercalation process. The properties of the nanocomposites obtained were quite close to the aerosilica-filled silicone rubber. Song et al. [38] prepared high performance nanocomposites consisting of a polyurethane elastomer and organoclay. An increase of 150% in both tensile strength and strain was observed and the fatigue properties were also improved. Pramanik et al. [39–41] used the solution method to obtain thermoplastic elastomer/clay nanocomposites. The tensile strength was doubled with 4 wt% organophilic clay loading and the thermal decomposition temperature was higher by about 34 °C [41].

Economic and environmental concerns lead to the development of new materials from renewable and inexpensive resources such as plant oils. The main composition of plant oil is triglyceride as shown in Fig. 1. Triglyceride based polymers have been developed and applied to structural materials as well as utilized as toughening agents [42,43]. A series of bio-based materials, such as pressure sensitive adhesives (PSA) [44], sheet molding composites (SMC) [45], elastomers [46–49], coatings [50], foams [51], etc. were developed from soybean oils by the ACRES (Affordable Composites from Renewable Resources) group at the University of Delaware. Tsujimoto et al. [52] and Uyama et al. [53] developed green nanocomposites consisting of plant oils and clay. Epoxidized plant oil was cured in the presence of organophilic montmorillonite to produce triglyceride–clay nanocomposites. A green nanocomposite coating was also developed by them. The hardness and mechanical properties were improved and good flexibility was shown as well as high biodegradability. Lu et al. [54] calculated the solubility parameters of the functionalized triglycerides and clay organic modifier and proved their miscibility. Flexural modulus and thermal stability improvement were observed. Liu et al. [55,56] prepared epoxidized soybean oil/clay nanocomposites by the extrusion solid freeform fabrication method. They reported that these nanocomposites could possess a variety of properties, ranging from elastomers to rigid plastics [55,56]. Green nanocomposites have also been prepared from cellulose acetate bio-plastic and clay and can be a substitute for polypropylene–clay nanocomposites for application in the automotive and transportation industries [57,58].

With proper miscibility, the polymer infiltrates into clay galleries in the exfoliated and intercalated structures as shown in Fig. 2. Clay disperses uniformly in the exfoliated state. Clay bundles are separated into individual layers and the clay layers are dispersed in the polymer matrix randomly. In the intercalated structure, the clay layers expand but still form an ordered structure. This structure is very similar to the polyurethane structure in which the hard sections form crystalline domains and work as physical crosslinks. Therefore, in the intercalated structure, it is possible that the nanoclay generates a physically crosslinked network which can have useful properties.

In previous papers [46–49], we showed that a bio-based elastomer from soybean oil was developed. Acrylated oleic methyl ester (AOME) synthesized from high oleic triglycerides can undergo free radical polymerization and form a high molecular weight linear polymer [44,59,60]. To obtain the elastic properties, ethylene glycol dimethacrylate (EGDMA) was used to crosslink the polymer *in situ*. The mechanical and thermal properties can be improved by adding methyl methacrylate (MMA) to modify the molecular structure of the rubber chain. In this work, organically modified clay was introduced to the elastomer network by *in situ* polymerization. A partially exfoliated structure was observed. The characterization of the clay/elastomer hybrid shows the changes in mechanical and thermal properties. The network structure was studied and related to these changes. A percolated filler network was formed and the crosslink density varied due to the addition of clay. Biodegradability of nanoclay filled samples was studied as well. Therefore, synthesis and characterization of nanoclay filled bio-based elastomers are the main focus of this paper.

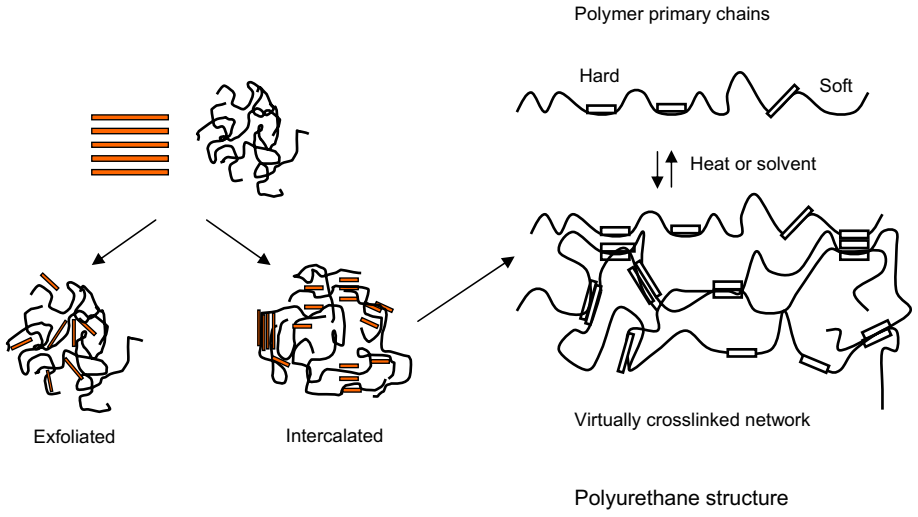

Fig. 2. Structure of polymer layered silicate and polyurethane. (The intercalated structure has some similarity with the polyurethane structure.)

2. Experimental

2.1. Preparation of clay/elastomer hybrid

There are four ways to synthesis polymer–clay nanocomposites: exfoliation–adsorption, *in situ* intercalative polymerization, melt intercalation and template synthesis [3]. In this work, *in situ* intercalative polymerization was used. Cloisite®15A, Cloisite®20A, Cloisite®25A, Cloisite®93A and Cloisite®30B were obtained from Southern Clay Products. They are nanoclays modified by different organic modifiers to render the clay from hydrophilic to organophilic. The information about the organic modifiers is listed in Table 1. Different ratios of clay were mixed with AOME (synthesized according to Bunker and Wool [59] as shown in Fig. 1) by mechanical stirring for 24 h. Cobalt naphthenate (CoNap) (0.8 wt%) activator (Witco Corp.) and 3 wt% Trigonox 239A (cumyl hydroperoxide in solution, Akzo Nobel) were then added. The mixture was purged with nitrogen for 5 min to prevent the oxygen free radical inhibition and then cured between gaskets made from silicone at room temperature. MMA (Specialty Polymer, Inc.) and EGDMA (Specialty Polymer, Inc.) were added in some samples before curing to modify the properties and crosslink density of the final elastomer.

Table 1
Information on different organoclays and XRD peak values of pure organoclays and poly(AOME) infiltrated organoclays

Clay type	Organic modifier	d_{001} (nm) peak of layered silicate	d_{001} (nm) peak of nanocomposites	Δd (nm)
Cloisite®15A	2M2HT	3.15	4.3	1.15
Cloisite®20A	2M2HT	2.42	4.2	1.78
Cloisite®93A	M2HT	2.36	3.6	1.24
Cloisite®30B	MT2EtOH	1.85	3.8	1.95

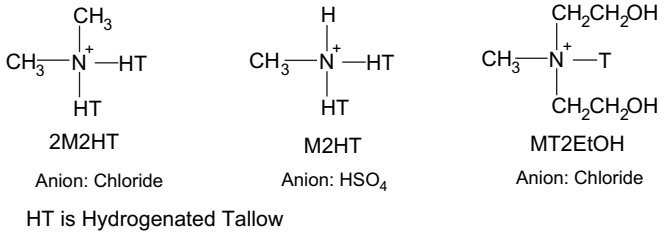

2.2. Characterization

2.2.1. Morphology and network structure

The morphology of the nanocomposite was measured by wide-angle X-ray diffraction (XRD) and transmission electron microscopy (TEM). XRD was performed on a Philips X'Pert diffractometer with Cu Kα radiation (40 kV, 40 mA) in the 2θ range of 1°–10°. TEM was carried out on JEOL2010 FX electron microscope on 60 nm thick section. The samples were cryo-microtomed from the cured sample at −50 °C. The fracture samples were examined using a JEOL JSM-7400F Field Emission Scanning Microscope with voltage of 1.0 kV. The surfaces were sputter-coated with a thin layer of gold to make the surface conductive. The degraded surface was studied on a Leitz Compound Optical Microscope.

The crosslink density was measured by a solvent swelling test. The swelling test was conducted in water, cyclohexane, MMA, toluene, benzene, chloroform, acetone and acrylic acid. All solvents except MMA are obtained from Fisher Scientific and used without any further treatment. The control dry weight, m_o, is 1 g. The sample was immersed in 10 ml solvent. The weight of the sample was measured every 24 h until equilibrium mass was obtained. Crosslink density was calculated by the Flory–Rehner's equations.

2.2.2. Mechanical and thermal properties

Tensile strength and elongation at break were tested on an Instron 4210 according to ASTM D-412. The samples were cut into dumbbell shape according to ASTM D 3182. A cross-head speed of 10 mm/min was used.

The glass transition temperature was determined by differential scanning calorimetry (TA Instruments Q100) at a heating rate of 10 °C/min in nitrogen atmosphere; a ramp from −90 °C to 25 °C was used. Sample of 10 mg was used for each measurement. Thermal stability was studied on a TA instrument Thermogravimetric Analyzer Q500. Helium was used as the purging gas. Sample of 2–3 mg was heated from room temperature to 700 °C at a heating rate of 10 °C/min.

2.2.3. Biodegradability

Biodegradability of the elastomers was studied by the soil burial method, as described by Goheen and Wool [61]. Samples were buried in garden soil and the soil was kept at room temperature with 50% moisture. Samples were removed from the soil at regular time intervals of 15 days and washed with distilled water to remove the surface soil. The samples were weighed after drying in the vacuum oven at 40 °C. The weight loss was recorded. The surfaces of the degraded samples were studied by optical microscopy.

3. Results and discussion

3.1. Organic modifier selection

If two systems are miscible with each other, the solubility parameters of these two systems are similar. Lu et al. successfully selected organoclay for functionalized plant oils by comparing the solubility parameter of the polymer with the nanoclays [54] and a similar approach was used here. The Hoy model [62] and the Hoftyzer–van Krevelen [63] model were used to predict the solubility parameter of poly(AOME) and organic clay modifiers. The calculated values are shown in Table 2 and the average values of these two models, which have increased accuracy, are shown in Table 2 as well. Cloisite®30B has a solubility parameter of 20.09. This value is very close to the calculated solubility parameter of poly(AOME), which is 19.86. Therefore, Cloisite®30B is more miscible with poly(AOME). Samples with 3 wt% of each kind of Cloisite® were prepared via *in situ* intercalation method and characterized by XRD as shown in Fig. 3. The peak values of each XRD curve are recorded in Table 1. The interaction between organic modifier and polymer determines the degree of intercalation. Cloisite®15A has the largest original layer distance and largest layer distance after intercalation. However, the layer distance change is the smallest which indicates that fewer polymer chains have infiltrated into the clay layers in Cloisite®15A. Cloisite®30B, which has the largest Δd value, has more polymer chains intercalated and is the most miscible one with poly(AOME). This confirms the theoretical calculation. The miscibility of Cloisite®30B and poly(AOME) may be due to the formation of hydrogen bonding between the hydroxyl groups in Cloisite®30B and carbonyls in poly(AOME) [64].

Table 2
Solubility parameters of poly(AOME) and organoclays predicted by Hoy model and Hoftyzer–van Krevelen model

Material	Hoy	HvK	Ave
Poly(AOME)	19.89	19.83	19.86
Cloisite®30B	20.17	20.01	20.09
Cloisite®15A/20A	17.76	17.28	17.52
Cloisite®93A	18.29	17.25	17.77

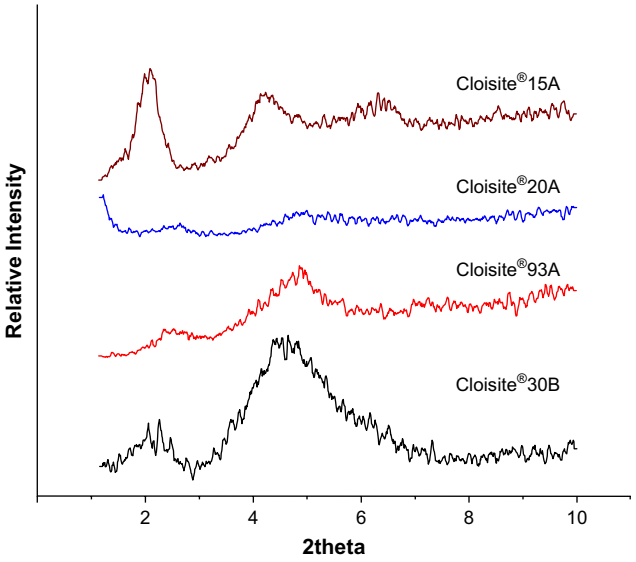

Fig. 3. XRD profiles for and poly(AOME) loaded with 3 wt% Cloisite®15A, Cloisite®20A, Cloisite®93A, and Cloisite®30B.

3.2. Morphology

XRD curves for samples with 1–15 wt% Cloisite®30B are shown in Fig. 4. If the clay and polymer are immiscible, the basal reflection does not change upon blending with the polymer. If intercalation occurs, the finite layer expands and results in a new basal reflection that corresponds to the larger gallery height. Cloisite®30B has only one peak at 4.77°. The polymer layered silicates have two peaks, while the polymer itself is amorphous and has no diffraction peak. One is in the same range as Cloisite®30B. The other appears at a lower diffraction angle around 2°. The peak shift to the lower diffraction angle

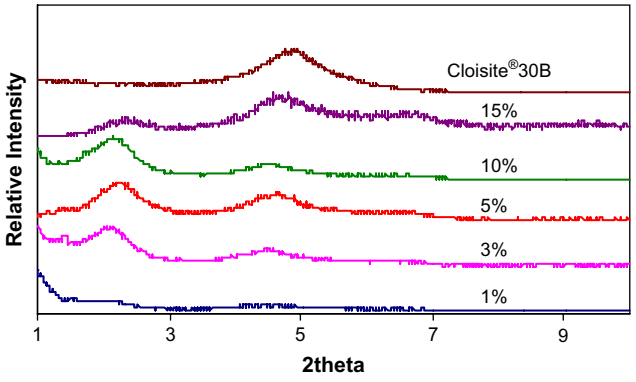

Fig. 4. XRD profiles for pure Cloisite®30B and poly(AOME) loaded with 15 wt%, 10 wt%, 5 wt%, 3 wt% and 1 wt% Cloisite®30B. (Polymer samples contain 5 wt% MMA and 1 wt% EGDMA.)

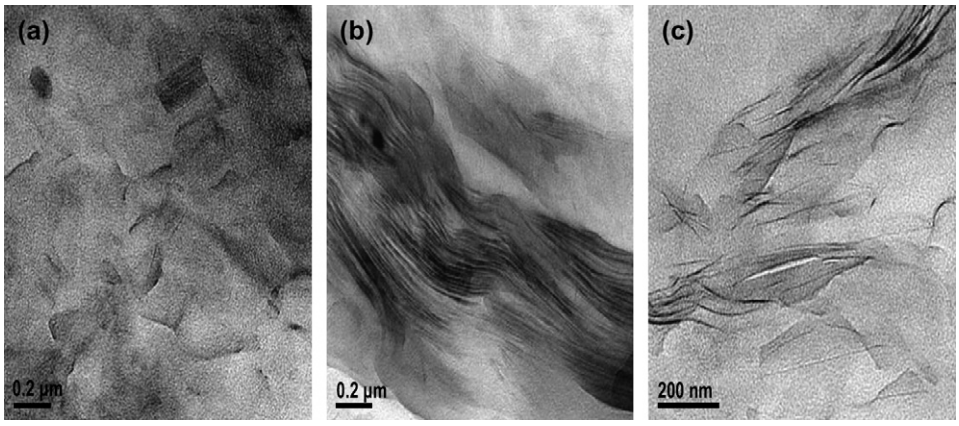

Fig. 5. TEM of 5 wt% Cloisite®30B loaded AOME elastomer: (a) low magnification, (b) intercalated structure, and (c) exfoliated structure. (The elastomer samples contain 5 wt% MMA and 1 wt% EGDMA.)

indicates the intercalation of polymers into clay layers and this phenomenon is obvious in samples with up to 10 wt% clay loading. The area under the peak can qualitatively identify the amount of the clay with certain spacing. With the increase of the clay ratio, the peak height at the low diffraction angle decreases. So the degree of exfoliation depends on the clay ratio. Quantitative analysis by X-ray diffraction has been studied by many researchers on clay minerals based on the principle that the intensity of a diffraction peak from a particular mineral is related to the abundance of that mineral in a mixture [65–70]. However, to achieve a precise result, quantitative analysis is difficult. Sample length, sample thickness, sample position and homogeneity, which influence the accuracy of the analysis, are very hard to control especially when the reflection angle is low ($2\theta < 10^\circ$) and the selected analytical peaks are far from each other [71]. The 2θ range in this study is between 0 and 10° and the attempt to analyze the data quantitatively results in too many errors. Therefore, only qualitative analysis is carried out in this research. In contrast to XRD, TEM is a more direct method to observe the intercalation and the TEM pictures for a sample with 5 wt% Cloisite®30B are shown in Fig. 5. Fig. 5(a) is taken at low magnification and indicates the distribution of clay in the polymer matrix. The clay is quite well dispersed though there are still some aggregates. In most area, the polymers infiltrate into the clay layers but the ordered structure remains. Clay bundles are shown in Fig. 5(b). In addition to the intercalated structure, in some area, an exfoliated structure is also shown as in Fig. 5(c). The clay is dispersed uniformly in the polymer matrix and not aligned anymore. XRD and TEM analyses confirm the formation of nanocomposites.

3.3. Mechanical properties

Nanoclay dramatically increases the tensile strength of the elastomer. A set of samples with 5 wt% MMA, 1 wt% EGDMA and various ratios of Cloisite®30B were prepared by the methods mentioned in Section 2. Cloisite®30B with 1 wt%, 3 wt%, 5 wt% and 10 wt% was used. Fig. 6 shows that the tensile strength linearly increases with the volume fraction of the clay. With 10 wt% clay, tensile strength changes from 0.08 MPa to 0.58 MPa which is a more than 600% increase. Even with as little as 1 wt% clay, which is only 0.5% by volume, the tensile strength increases almost 100%. Increases in tensile strength for conventional elastomers are always accompanied by a decrease in resilience. However, in this nanoclay filled elastomer, the elongation increases as well as the tensile strength as shown in Fig. 7. The elongation of pure elastomer is 85%, but with 1 wt% clay, the elastomer can be extended up to 121%. The increase levels off at high clay loadings but still an elongation of 190% is observed when the clay loading is 10 wt%. MMA effects on the mechanical properties of pure AOME based elastomers have been studied and it was shown that a certain ratio of MMA can improve the network perfection [49,72]. The MMA effect on the nanoclay filled elastomers was studied

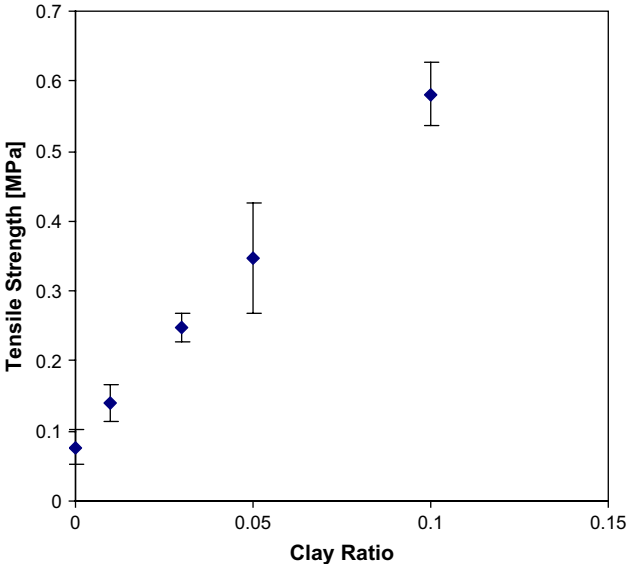

Fig. 6. Tensile strength of samples without nanoclay, with 1 wt%, 3 wt%, 5 wt%, and 10 wt% Cloisite®30B. (All elastomer samples contain 5 wt% MMA and 1 wt% EGDMA.)

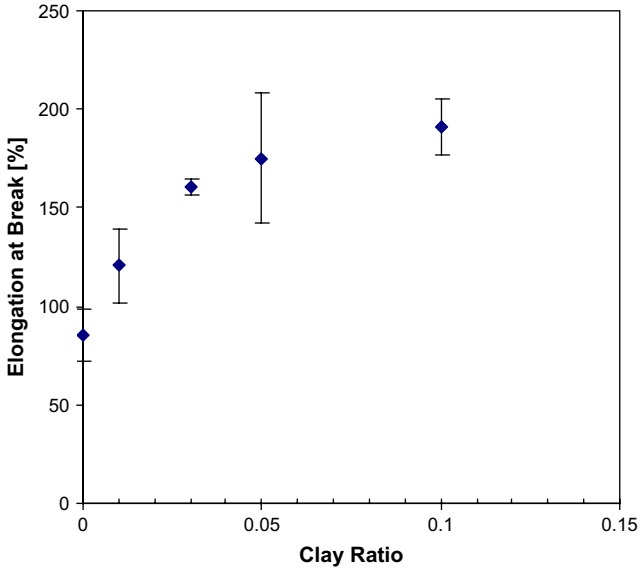

Fig. 7. Maximum elongation of elastomers samples without nanoclay, with 1 wt%, 3 wt%, 5 wt% and 10 wt% Cloisite®30B. (All elastomer samples contain 5 wt% MMA and 1 wt% EGDMA.)

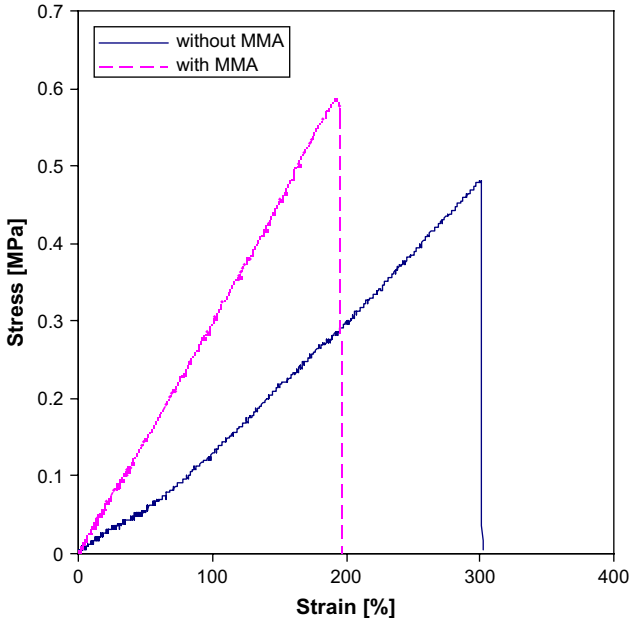

Fig. 8. Stress–strain curves of elastomers without MMA and with 5 wt% MMA. (Both samples contain 1 wt% EGDMA and 10 wt% Cloisite®30B.)

as well. Mechanical properties of the sample with 5 wt% MMA are compared with the sample without MMA in Fig. 8. Both samples are loaded with 10 wt% Cloisite®30B. With 5 wt% MMA, the tensile strength increases but the maximum strain decreases. This is probably because the addition of MMA facilitates the chemical crosslinking. MMA is a smaller molecule when compared with the long fatty acids, so it is easier to react with EGDMA. The addition of MMA dilutes the density of the long branches and reduces the steric hindrance. Therefore, the crosslinking becomes easier.

3.4. Crosslink density and network perfection

Crosslink density of the set of samples with different ratios of Cloisite®30B was tested by the swelling test and calculated using Flory—Rehner's equation [73]:

$$v = -\frac{\ln(1-v_r) + v_r + \chi v_r^2}{V_1\left(v_r^{1/3} - 0.5v_r\right)} \tag{1}$$

where v_r is the volume fraction of the polymer in the mixture, χ is the polymer–solvent interaction parameter and V_1 is the molar volume of the solvent. V_r and χ are obtained by the following equations [74]:

$$V_r = \frac{\text{weight of rubber/density of rubber}}{\text{weight of rubber/density of rubber} + \text{weight of solvent/density of solvent}} \tag{2}$$

$$\chi = \chi_H + \chi_s = V_1(\delta_1 - \delta_2)^2/RT + 0.34 \tag{3}$$

where χ_H and χ_s are the enthalpic and entropic components of χ, δ_1 and δ_2 are the solubility parameters of polymer and solvent, respectively. The solubility parameter of the polymer is obtained by fitting the swelling coefficients of the polymer in various solvents. The swelling coefficient Q is defined by [75]:

$$Q = \frac{m - m_0}{m_0} \times \frac{1}{\rho_s} \tag{4}$$

where m is the weight of the most swollen sample, m_0 is the weight of the dry sample and ρ_s is the density of the swelling solvent. The swelling coefficient was then plotted as a function of solubility parameter and the maximum in $Q(\delta)$ curve gives the solubility parameter of the polymer, δ_1. The solvent which has the closest δ value is considered a good solvent and its swelling data are used for the calculation of the crosslink density by Eq. (1). The swelling coefficient, Q, was calculated and plotted against the solubility parameter δ of various solvents as shown in Fig. 9. Poly(AOME) has a maximum swelling at $\delta = 18.6$ which is very close to the solubility parameter of benzene, $\delta = 18.8$. Therefore, benzene is a good solvent for poly(AOME) and the swelling measurement results in benzene were used to calculate the crosslink density.

The results of crosslink density are shown in Fig. 10. The crosslink density increases with modulus according to rubber elasticity theory. So the higher modulus value in the clay filled rubber should indicate a higher crosslink density. Using the modulus data obtained from the tensile test, the crosslink density, ν, was calculated by:

$$\nu = \frac{G}{RT} \tag{5}$$

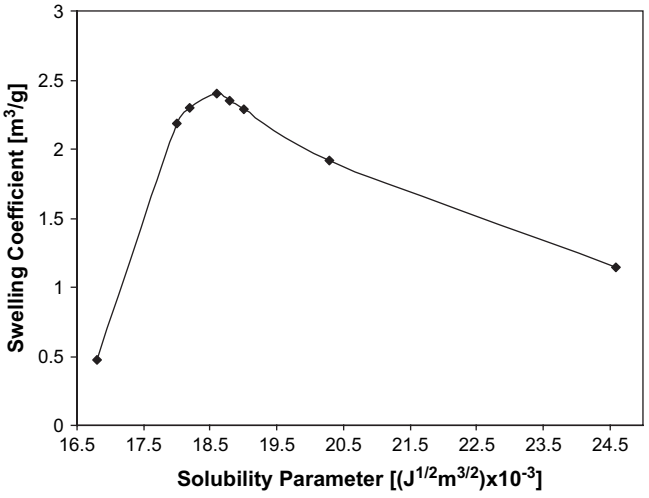

Fig. 9. Swelling coefficient of poly(AOME) in solvents with different solubility parameters.

where G is the shear modulus, R is the ideal gas constant, and T is the absolute temperature. The results are shown in Fig. 10 as well. The crosslink density from the swelling test shows a lower crosslink density at clay loading of 3% and 5% than the pure elastomer. As shown in Fig. 5, the morphology of the nanoclay filled elastomer is not uniform. The clay distribution varies from exfoliation to intercalation. Exfoliated clay will not contribute to the crosslink density but the interaction between the organic modifier and polymer chains has some reinforcement effect and will contribute to the increase in the modulus. In the intercalated state, the clay bundles may form physical crosslinks and result in an increase in the total crosslink density and contribute to the modulus increase. However, during the swelling test, a portion of intercalated clays, especially the bundles in which the layers are far apart, may open due to the swelling of the polymer chain as shown schematically in Fig. 11. XRD curves in Fig. 4 show that the average distance between clay layers varies with clay ratios. In the 10 wt% clay filled sample, clay bundles are more crowded, the interactions are stronger and the bundles are less easy to separate during swelling. The measured crosslink density is the largest among the three clay loaded samples. Therefore, the crosslink density from swelling test is actually the chemical crosslink density with part of the physical crosslinks instead of the total apparent crosslink density. The lower crosslink density in 3 wt% and 5 wt% clay filled samples may also indicate that the loading of the clay hinders the formation of chemical crosslinks and physical crosslinks are formed by the clay bundles.

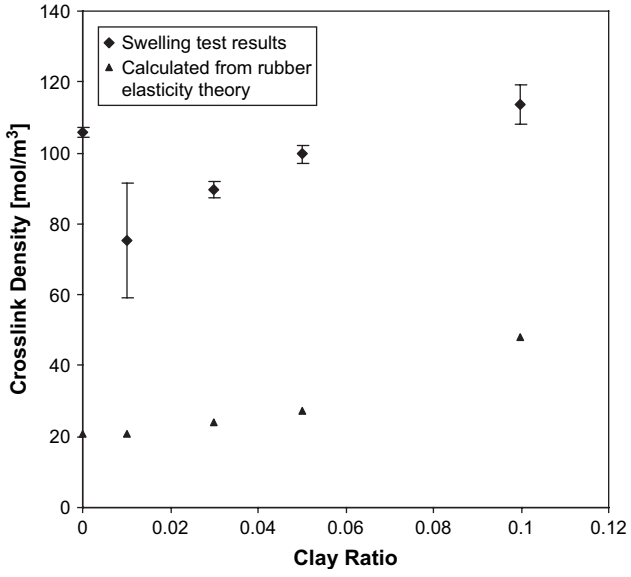

Fig. 10. Crosslink density of AOME elastomers without nanoclay, with 1 wt%, 3 wt%, 5 wt% and 10 wt% Cloisite®30B (All elastomer samples contain 5 wt% MMA and 1 wt% EGDMA.)

Percolation theory can be used to predict the mechanical properties [76]. It studies the formation and structure of clusters in a large lattice whose sites or bonds are present with a certain probability. It can be calculated numerically by Monte Carlo simulations or other techniques [77]. The percolation fraction of bonds that must be broken to cause fracture in the network can be calculated from [76]:

$$[P - P_c] = \frac{U_f}{vD_0} \tag{6}$$

where P is the occupation probability of the bonds in the lattice. P_c is the percolation threshold, which is the probability for which a continuous path of nearest neighbors appears from one side of the lattice to the other side. U_f is the fracture energy of the elastomer, which can be obtained by the area under stress–strain curve. D_0 is the bond dissociation energy and is 348 kJ/mol for carbon–carbon bonds. Fig. 12 gives the calculated $[P - P_c]$ value. With increasing clay content, $[P - P_c]$ increases almost linearly when the clay ratio is less than 5% but levels off at 10% clay loading. Addition of the clay increases the perfection of the network by connecting the free chains together and forms physical crosslinks. However, the network is still imperfect as indicated by the low $[P - P_c]$ value and that is the reason for the low mechanical properties.

3.5. Thermal stability and glass transition temperature

TGA data in Table 3 indicate the effects of nanoclay on the thermal stability of the polymer. The onset of thermal decomposition of nanoclay filled samples shifted significantly to higher temperatures. T_i in Table 3 is the temperature where the sample has 3% weight loss. With the loading of the clay, T_i increases. Without clay, T_i is 133 °C and with 3% clay T_i increases by 12 °C. This is due to the hindered diffusion of volatile decomposition products within the nanocomposites. However, the temperature at which the decomposition rate reaches the maximum decreases with the loading of the clay. The pure elastomer sample decomposed fastest at 357 °C. For clay loaded samples, the fastest decomposition occurred in the range of 350 °C and did not change much with clay ratios. The different effects of clay in different stages of thermal degradation can be explained as the following. The clay acts as

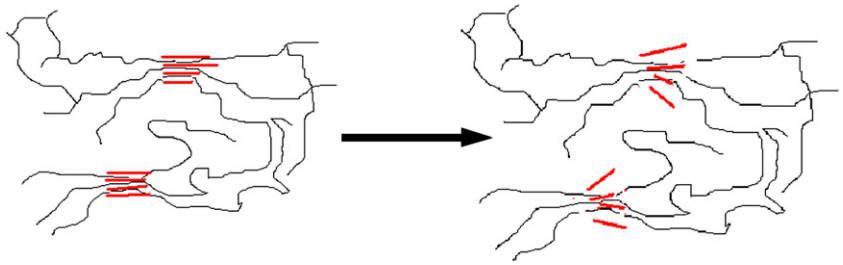

Fig. 11. Schematic of physical crosslink opening during swelling.

a heat barrier and enhances the overall thermal stability of the system as well as assists in the formation of char after thermal decomposition [78]. In the early stage of thermal decomposition, the clay shifted the decomposition to a higher temperature. However, the layered structure can also hold accumulated heat, which can be used as a heat source to accelerate the decomposition process. In addition, it is also possible that clay minerals behave like catalyst and form active sites in the polymer. Therefore the thermal stability of the nanocomposites is decreased.

The glass transition temperature of the poly(AOME) with 1 wt% EGDMA elastomer is −60 °C. To eliminate the effect of MMA on the glass transition temperature, another set of samples with 1 wt% EGDMA and various ratios of clays were prepared without MMA. Fig. 13 shows clay effects on glass transition temperature. The data are the average values of three measurements. Samples of a certain clay ratio were cut from the same sheet of elastomer. The samples with clay have a similar T_g around −50 °C, though the one with 10% clay is slightly lower. The clay bundles restrict the molecular motions and enhance T_g but at the same time the organic modifier group may bring some plasticizer effects to reduce T_g. These dual effects make the clay effects on glass transition temperature very complicated. It is also observed that the standard deviation of the data is getting larger with clay ratio. T_g of the sample with 10% clay varies from −48 °C to −56 °C. The large error bar indicates that the sample is heterogeneous and T_g depends on the clay dispersion in the polymer matrix.

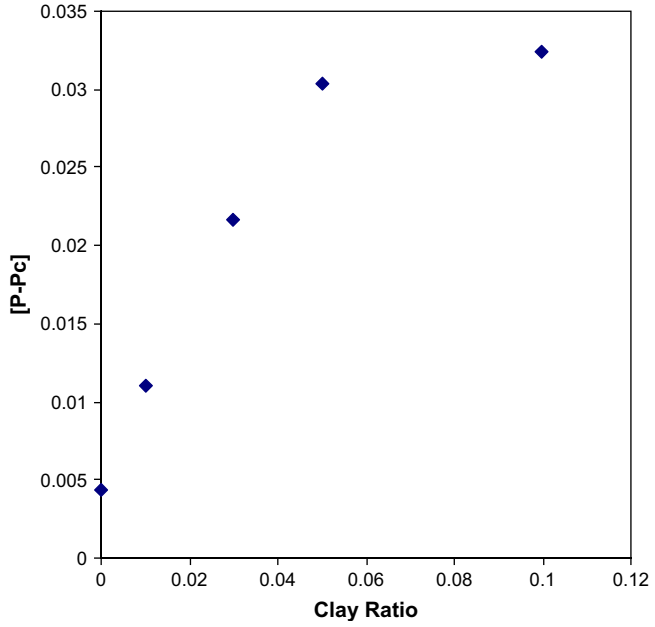

Fig. 12. Network perfection of elastomers without nanoclay, with 1 wt%, 3 wt%, 5 wt% and 10 wt% Cloisite®30B. (All elastomer samples contain 5 wt% MMA and 1 wt% EGDMA.)

3.6. Biodegradability

Weight loss of samples with different clay ratios is plotted as a function of time in Fig. 14. Weight loss was larger in nanoclay filled samples, but the degradation was not proportional to the clay content. The 3% clay loaded sample has a similar weight loss as the sample with 10% clay in the first 45 days and an even larger value afterward. All the samples have a large initial degradation rate and slows down later. Pictures were taken on the biodegraded surface of the poly(AOME) elastomer with and without clay under different magnifications. Fig. 15 shows the AOME elastomers with 5 wt% MMA and 1 wt% EGDMA but without clay. The sample with or without clay generates a similar degraded surface. Some interesting structures were observed at high magnifications. Pearl-like and seashell-like structures were observed and rainbow colors were shown together with these interesting structures. The mechanism for the biodegradation needs further study, but the abnormal structures are believed to be related to degradation by different microorganisms. The increase in the rate of biodegradation has also been found in the study of poly(L-lactic acid) nanocomposites [79] and polylactide–clay, poly(butylenes succinate)–clay nanocomposites [80–82]. The type of organoclay and loading level affect biodegradation kinetics [83]. This suggests that the biodegradation can be finely tuned. The combination of improved mechanical properties and controlled biodegradability makes these materials attractive for biomedical and packaging applications.

Table 3
TGA data of poly(AOME) elastomers without Cloisite®30B, with 3 wt%, 5 wt%, and 10 wt% Cloisite®30B

Clay wt%	T_i (°C)	T_{max} (°C)
No clay	133	357
3% Clay	145	349
5% Clay	145	350
10% Clay	150	352

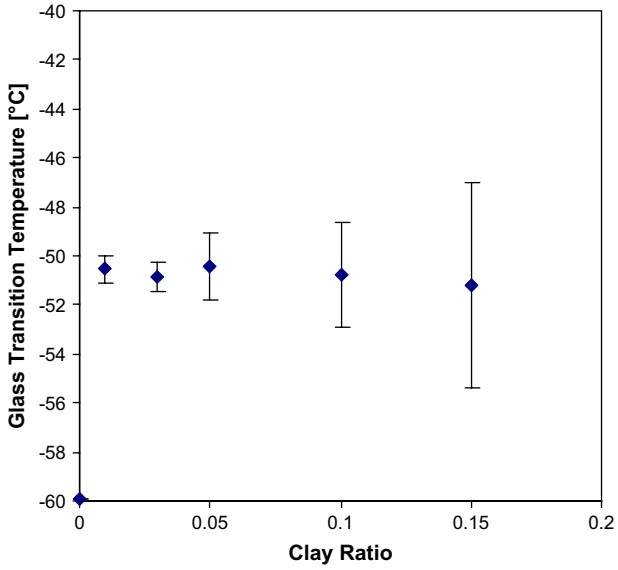

Fig. 13. Glass transition temperature of AOME elastomers without nanoclay, with 1 wt%, 3 wt%, 5 wt% and 10 wt% Cloisite®30B. (All elastomer samples contain 1 wt% EGDMA.)

4. Conclusions

A nanoclay filled AOME elastomer was successfully synthesized from soybean oil. The nanoclay dramatically improved the properties of the bio-based elastomers. Solubility theory predicted that Cloisite®30B, which has an organic modifier (methyl, tallow, bis-2-hydroxyethyl, quaternary ammonium), has a similar solubility parameter to poly(AOME) and is more miscible with the resin than the other organoclays. XRD and TEM analyses showed the resin mixed with the nanoclay on the nano-scale and nanocomposites were formed. The morphology varied with different loadings of nanoclays. Good intercalated structure was obtained with up to 10 wt% clay loading. The mechanical properties were notably improved. The tensile strength increased as well as the elongation with the loading of the clay. Percolation theory predicted that the network is still far from perfect and the loading of the clay increases the perfection of the network. The onset of thermal decomposition was hindered by the clay. The glass transition temperature depends on the dispersion of the nanoclay in the nanocomposites. Preliminary soil burial tests show that poly(AOME) elastomer is biodegradable. Nanoclay improves the biodegradation and the mechanism is still under study.

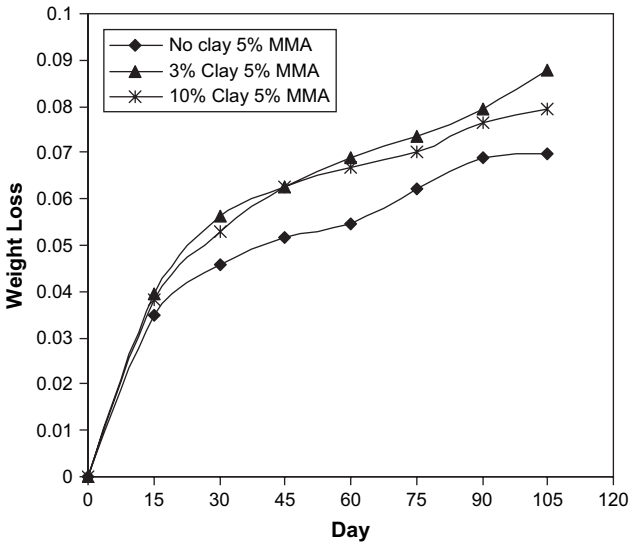

Fig. 14. Weight loss change of AOME elastomers (without nanoclay, with 3 wt% and 10 wt% Cloisite®30B with time. (All samples contain 5 wt% MMA and 1 wt% EGDMA.)

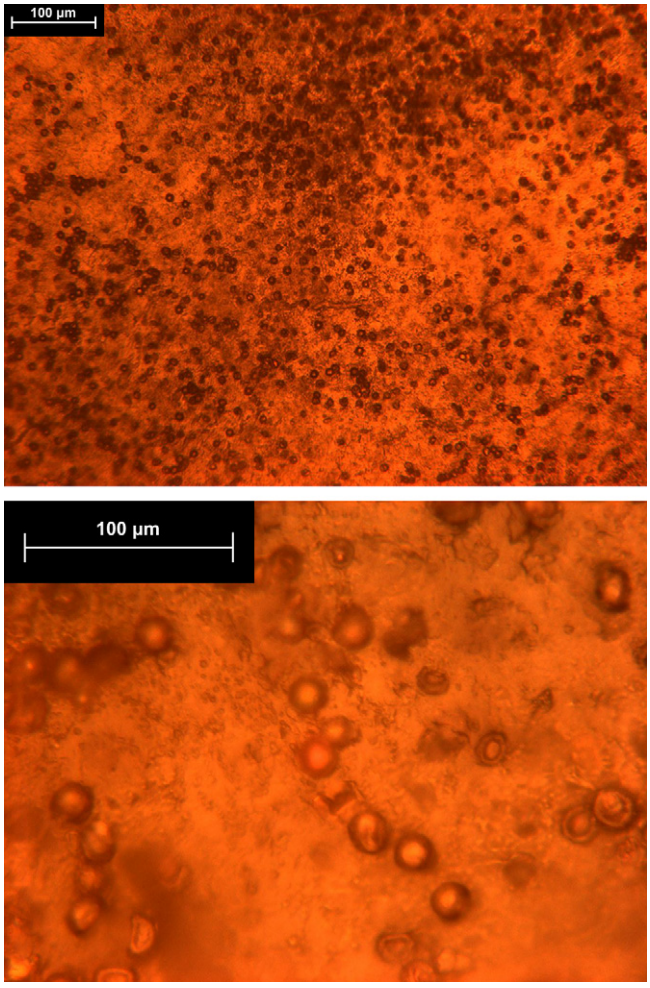

Fig. 15. Optical microscope pictures of biodegraded surface of AOME elastomer with 5 wt% MMA and 1 wt% EGDMA.

References

[1] Morton M, editor. Rubber technology. New York: Van Nostrand Reinhold Company; 1987.
[2] Fukushima Y, Inagaki S. J Inclusion Phenom 1987;5(4):473–82.
[3] Alexandre M, Dubois P. Mater Sci Eng R 2000;28(1–2):1–63.
[4] Salahuddin NA. Polym Adv Technol 2004;15(5):251–9.
[5] Lan T, Pinnavaia TJ. Chem Mater 1994;6(12):2216–9.
[6] Ratna D, Manoj NR, Varley R, Raman RKS, Simon GP. Polym Int 2003;52(9):1403–7.
[7] Pinnavaia TJ, Lan T, Wang Z, Shi HZ, Kaviratna PD. Clay-reinforced epoxy nanocomposites: synthesis, properties, and mechanism of formation. Nanotechnology 1996;250–61.

[8] Ratna D, Becker O, Krishnamurthy R, Simon GP, Varley RJ. Polymer 2003;44(24):7449–57.
[9] Kang JH, Lyu SG, Sur GS. Polymer Korea 2000;24(4):571–7.
[10] Daniel IM, Miyagawa H, Gdoutos EE, Luo JJ. Exp Mech 2003; 43(3):348–54.
[11] Lee CR, Ihn KJ, Gong MS. Polymer Korea 2003;27(4):392–5.
[12] Kornmann X, Lindberg H, Berglund LA. Polymer 2001;42(4):1303–10.
[13] Lan T, Kaviratna PD, Pinnavaia TJ. Chem Mater 1994;6(5):573–5.
[14] Delozier DM, Orwoll RA, Cahoon JF, Johnston NJ, Smith JG, Connell JW. Polymer 2002;43(3):813–22.
[15] Yano K, Usuki A, Okada A, Kurauchi T, Kamigaito O. J Polym Sci Part A Polym Chem 1993;31(10):2493–8.
[16] Yano K, Usuki A, Okada A. J Polym Sci Part A Polym Chem 1997; 35(11):2289–94.
[17] Kim KY, Lim HJ, Park SM, Lee SJ. Polymer Korea 2003;27(4): 377–84.
[18] Tseng CR, Wu JY, Lee HY, Chang FC. J Appl Polym Sci 2002;85(7): 1370–7.
[19] Qutubuddin S, Fu XA, Tajuddin Y. Polym Bull 2002;48(2):143–9.
[20] Fu X, Qutubuddin S. Mater Lett 2000;42(1–2):12–5.
[21] Chen AM, Tian Y, Han B, Ji GD, Wu SS, Shen J. Acta Polym Sin 2003;(4):591–4.
[22] Ma JS, Qi ZN, Zhang SF. Acta Polym Sin 2001;(3):325–8.
[23] Wang Z, Pinnavaia TJ. Chem Mater 1998;10(12):3769–71.
[24] Zhang YQ, Lee JH, Rhee JM, Rhee KY. Compos Sci Technol 2004;64(9):1383–9.
[25] Ma JS, Qi ZN, Hu YL. J Appl Polym Sci 2001;82(14):3611–7.
[26] Hasegawa N, Okamoto H, Kawasumi M, Usuki A. J Appl Polym Sci 1999;74(14):3359–64.
[27] Xu LQ, Lee LJ. Polym Eng Sci 2005;45(4):496–509.
[28] Phang IY, Pramoda KP, Liu TX, He CB. Polym Int 2004;53(9): 1282–9.
[29] Nazare S, Kandola BK, Horrocks AR. Polym Adv Technol 2006;17(4): 294–303.
[30] Kornmann X, Berglund LA, Sterte J, Giannelis EP. Polym Eng Sci 1998;38(8):1351–8.
[31] Kojima Y, Fukumori K, Usuki A, Okada A, Kurauchi T. J Mater Sci Lett 1993;12(12):889–90.
[32] Lopez-Manchado MA, Herrero B, Arroyo M. Polym Int 2003;52(7): 1070–7.
[33] Arroyo M, Lopez-Manchado MA, Herrero B. Polymer 2003;44(8): 2447–53.
[34] Lopez-Manchado MA, Arroyo M, Herrero B, Biagiotti J. J Appl Polym Sci 2003;89(1):1–15.
[35] Vu YT, Mark JE, Pham LH, Engelhardt M. J Appl Polym Sci 2001; 82(6):1391–403.
[36] Zhang LQ, Wang YZ, Wang YQ, Sui Y, Yu DS. J Appl Polym Sci 2000; 78(11):1873–8.
[37] Wang SJ, Long CF, Wang XY, Li Q, Qi ZN. J Appl Polym Sci 1998; 69(8):1557–61.
[38] Song M, Hourston DJ, Yao KJ, Tay JKH, Ansarifar MA. J Appl Polym Sci 2003;90(12):3239–43.
[39] Pramanik M, Srivastava SK, Samantaray BK, Bhowmick AK. Macromol Res 2003;11(4):260–6.
[40] Pramanik M, Srivastava SK, Samantaray BK, Bhowmick AK. J Appl Polym Sci 2003;87(14):2216–20.
[41] Pramanik M, Srivastava SK, Samantaray BK, Bhowmick AK. J Polym Sci Part B Polym Phys 2002;40(18):2065–72.
[42] Khot SN, Lascala JJ, Can E, Morye SS, Williams GI, Palmese GR, et al. J Appl Polym Sci 2001;82(3):703–23.
[43] Wool RP, Sun XS. Bio-based polymers and composites. Burlington, MA: Elsevier; 2005.
[44] Bunker S, Staller C, Willenbacher N, Wool R. Int J Adhes Adhes 2003; 23(1):29–38.
[45] Lu J, Khot S, Wool RP. Polymer 2005;46(1):71–80.
[46] Zhu L, Wool RP. Abstra Papers Am Chem Soc 2004;228:U459.
[47] Zhu L, Wool RP. Elastomer from renewable resources: synthesis and characterization. Abstr Papers Am Chem Soc 2004.
[48] Zhu L, Wool RP. Acrylate rubber/organoclay hybrid nanocomposites from renewable resources. In: The 20th ASC technical meeting, Philadelphia, PA; 2005.
[49] Zhu L, Wool RP. Biodegradable elastomers from plant oils. In: The 230th ACS annual meeting, Washington, DC; 2005.
[50] Kulbick AL. Development of bio-based emulsion polymers for use in coating systems. Newark: Department of Chemical Engineering, University of Delaware; 2004.
[51] Bonnaillie LM. Method for fabrication of bio-based thermoset foam from acrylated epoxidized soybean oil. Newark: Department of Chemical Engineering, University of Delaware; 2004.
[52] Tsujimoto T, Uyama H, Kobayashi S. Macromol Rapid Commun 2003;24(12):711–4.
[53] Uyama H, Kuwabara M, Tsujimoto T, Nakano M, Usuki A, Kobayashi S. Chem Mater 2003;15(13):2492–4.
[54] Lu J, Hong CK, Wool RP. J Polym Sci Part B Polym Phys 2004;42(8): 1441–50.
[55] Liu ZS, Erhan SZ, Calvert PD. J Am Oil Chem Soc 2004;81(6):605–10.
[56] Liu ZE, Sevim Z, Jingyuan Xu. Polymer 2005;46:10119–27.
[57] Park HM, Liang XM, Mohanty AK, Misra M, Drzal LT. Macromolecules 2004;37(24):9076–82.
[58] Park HM, Misra M, Drzal LT, Mohanty AK. Biomacromolecules 2004; 5(6):2281–8.
[59] Bunker SP, Wool RP. J Polym Sci Part A Polym Chem 2002;40(4): 451–8.
[60] Bunker S. The synthesis and characterization of pressure sensitive adhesives from a fatty acid methyl ester. Newark: Department of Chemical Engineering. University of Delaware; 2003.
[61] Goheen SM, Wool RP. J Appl Polym Sci 1991;42:2691–701.
[62] Hoy KL. J Coated Fabrics 1989;19:53.
[63] Van Krevlen DW. Properties of polymers: their correlation with chemical structure. Amsterdam: Elsevier Science; 1997.
[64] Kalgaonkar RA, Jog JP. J Polym Sci Part B Polym Phys 2003;41(23): 3102–13.
[65] Reynolds RC, Distefano MP, Lahann RW. Clays Clay Miner 1992;40(3): 262–7.
[66] Reynolds RC. Clays Clay Miner 1986;34(4):359–67.
[67] Srodon J, Drits VA, McCarty DK, Hsieh JCC, Eberl DD. Clays Clay Miner 2001;49(6):514–28.
[68] Cody RD, Thompson GL. Clays Clay Miner 1976;24(5):224–31.
[69] Brindley GW, Kurtossy SS. Am Mineral 1962;47(9–10):1213.
[70] Brindley GW, Kurtossy SS. Am Mineral 1961;46(11–12):1205–15.
[71] Moore DM, Reynolds Jr RC. X-ray diffraction and the identification and analysis of clay minerals. 2nd ed. New York: Oxford University Press; 1997.
[72] Wool RP, Sun XS. Bio-based polymers and composites. Burlington, MA: Elsevier; 2005.
[73] Flory PJ. J Chem Phys 1950;18(1):108–11.
[74] Brydson JA. Rubbery materials and their compounds. Elsevier Applied Science; 1988.
[75] Sperling LH. Introduction to physical polymer science. John Wiley & Sons, Inc; 1992.
[76] Wool RP. J Polym Sci Part B Polym Phys 2005;43(2):168–83.
[77] Wool RP. Polymer interfaces. New York: Hanser & Gardner Press; 1995.
[78] Ray SS, Okamoto M. Prog Polym Sci 2003;28(11):1539–41.
[79] Schmidt D, Shah D, Giannelis EP. Curr Opin Solid State Mater Sci 2002;6(3):205–12.
[80] Ray SS, Yamada K, Okamoto M, Fujimoto Y, Ogami A, Ueda K. Polymer 2003;44(21):6633–46.
[81] Ray SS, Okamoto K, Okamoto M. Macromolecules 2003;36(7): 2355–67.
[82] Ray SS, Yamada K, Okamoto M, Ogami A, Ueda K. Chem Mater 2003; 15(7):1456–65.
[83] Chen B. Br Ceram Trans 2004;103(6):241–9.